Journal of Materials Chemistry

Cite this: J. Mater. Chem., 2012, 22, 14674

www.rsc.org/materials

PAPER

Development of highly luminescent and cytocompatible near-IR-emitting aqueous Ag_2S quantum dots†

Ibrahim Hocaoglu,[a] M. Natali Çizmeciyan,[a] Rengin Erdem,[b] Can Ozen,[b] Adnan Kurt,[c] Alphan Sennaroglu[ad] and Havva Yagci Acar*[ae]

Received 29th March 2012, Accepted 30th May 2012
DOI: 10.1039/c2jm31959d

Colloidally stable and highly luminescent near-IR emitting Ag_2S quantum dots (NIRQDs) were prepared by a very simple aqueous method using 2-mercaptopropionic acid (2MPA) as a coating. Emission of Ag_2S-2MPA NIRQDs can be tuned between 780 and 950 nm. These NIRQDs have photoluminescence quantum yields (PLQY) around 7–39% and exhibit excellent cytocompatibility even at 600 μg mL^{-1} in NIH/3T3 cells. With such improved properties, Ag_2S-2MPA NIRQDs have a great potential in practical bio-applications.

Introduction

Quantum dots, with their unique optical and electrical properties, initiated many developments in a variety of technology areas. The group II–VI semiconductors CdS, CdTe and CdSe are the most studied ones, and they emit in the visible region.[1–3] Lately, there is a tremendous demand for near infrared (NIR) emitting quantum dots (NIRQDs), especially in biological applications and in efficient solar energy conversion.[4]

In photovoltaic solar cells, expanding these systems to the NIR region is highly desirable in order to prevent heating of the device and to capture a broader range of the solar spectrum.[5] This can be best achieved with NIRQDs since most organic materials do not absorb in the NIR region.[5,6]

In biotechnology applications, QDs offer enormous advantages over organic fluorophores, with unmatched luminescence lifetime, higher sensitivity and a broad absorbance–narrow luminescence emission band, which enables excitation of multiple QDs at a single wavelength, and multiplexing. However, QDs that are excited in the UV and emit in the visible region are not that practical. Firstly, biological constituents, like water, hemoglobin and deoxyhemoglobin absorb and scatter light in the visible region (400–700 nm) and therefore have a quenching effect.[7–9] Secondly, living tissue (like collagen)[6] has significant autofluorescence in the visible region.[10] Thirdly, the penetration depth of visible light is limited.[10,11]

The near infrared range (700–900 nm) is considered as an appropriate diagnostic window for biological applications.[12,13] *In vitro* and *in vivo* bioimaging and biolabeling,[14] deep tissue imaging,[9] diagnostics[1] and photodynamic therapy[15] are some of the many potential bio-application areas for NIRQDs.

Some typical examples of NIRQDs reported in the literature are CdSeTe,[16] CdSeTe/Cd, CdHgTe/CdS,[17] CdTe/CdSe/ZnSe[18] and PbS.[9] There are a few NIRQDs that have been used successfully in *in vivo* imaging: Morgan *et al.*[19] used CdMnTe/Hg QDs as an angiographic contrast agent, Kim *et al.*[20] demonstrated imaging of sentinel lymph nodes in mice with CdTe/CdSe QDs, and Prasad *et al.*[21] used CdTe/ZnS QDs in the imaging of a PANC-1 tumor. However, apart from the imaging window consideration, toxicity is another important road-block in the practical use of QDs, especially for *in vivo* bio-applications. Elemental forms of cadmium, lead and mercury as well as their chalcogens are quite toxic.[22,23] Therefore, there is an urgent demand and a tremendous effort to decrease the cytotoxicity of QDs and/or to develop non-cytotoxic QDs. Although significant improvement in cytocompatibility is achieved through core–shell structures and PEGylation of Cd-based QDs, there is a growing effort towards the development of Cd-free QDs for bio-applications.[21,24]

Ag_2S has a band gap energy of 0.9 eV and is stable in the α-phase with a monoclinic crystal structure (α-Ag_2S).[25,26] Previously, Hirsch reported no significant toxicity of bulk Ag_2S.[27] Non-aqueous preparation of silver chalcogenide NIRQDs and their properties for potential applications have been recently documented in the literature.[22,28–30] These Ag_2X-NIRQDs (X: S, Se, Te) emit in the range of 690–1127 nm, but exhibit low

[a]*Koc University, Graduate School of Materials Science and Engineering, Rumelifeneri Yolu, Sarıyer, 34450 Istanbul, Turkey. E-mail: fyagci@ku.edu.tr; Fax: +90 2123381559; Tel: +90 2123381742*
[b]*Biotechnology Dept., Center of Excellence in Biomaterials and Tissue Engineering (BIOMATEN) and Central Laboratory, Middle East Technical University, Ankara, Turkey*
[c]*Teknofil, Inc., Zekeriyakoy, 34450 Istanbul, Turkey*
[d]*Koc University, Department of Physics, Rumelifeneri Yolu, Sarıyer, 34450 Istanbul, Turkey*
[e]*Koc University, Department of Chemistry, Rumelifeneri Yolu, Sarıyer, 34450 Istanbul, Turkey*

† Electronic supplementary information (ESI) available: TEM images of Ag_2S-2MPA nanoparticles, time dependent absorbance and luminescence spectra of particles synthesized at 30 and 90 °C, and absorbance spectra of particles prepared at different Ag : S and 2MPA : Ag ratios at 30 and 90 °C. See DOI: 10.1039/c2jm31959d

photoluminescence quantum yields (PLQY below 2%).[28,29] In addition, only the toxicity (almost nontoxic up to 50 μg mL^{-1}) of Ag_2Se NIRQDs has been reported and used for *in vivo* imaging.[31] Aqueous preparation methods for colloidal Ag_2S nanoparticles, relevant for biological applications, are quite rare in the literature. Castanon *et al.* prepared Ag_2S in aqueous media, but particles were at least 30 nm and no data on optical properties were available.[32] Considering the low band gap and potential for cytocompatibility, aqueous Ag_2S nanoparticles, especially those with improved luminescence, are one of the best candidates for NIRQDs for biological applications.[19,28]

Here, a one-step synthesis of 2-mercaptopropionic acid (2-MPA) coated aqueous Ag_2S NIRQDs was demonstrated (Scheme 1). The influence of reaction variables such as Ag : S and 2MPA : Ag ratios and reaction temperature on the optical properties of nanoparticles was investigated. For potential biological uses, the cytocompatibility of particles was investigated and *in vitro* imaging using NIH/3T3 cell lines was demonstrated.

Materials and methods

Materials

All reagents were analytical grade or highest purity. Silver nitrate ($AgNO_3$) was purchased from Sigma-Aldrich. Sodium sulfide (Na_2S) was purchased from Alfa-Aesar. 2-Mercaptopropionic acid (2-MPA), acetic acid (CH_3COOH), sodium hydroxide (NaOH), and 4% paraformaldehyde were purchased from Merck. LDS 798 near-IR laser dye was purchased from Exciton Inc. Milli-Q water (18 mΩ) was used as the solvent. DMEM medium (with 1.0 g L^{-1} glucose, stable L-glutamine, 3.7 g L^{-1} $NaHCO_3$, and phenol red), 10% fetal bovine serum and trypsin–EDTA were purchased from Biochrom AG, Germany. 1% penicillin–streptomycin antibiotic solution was purchased from HyClone, USA. Sodium 3′-[1-(phenylaminocarbonyl)-3,4-tetrazolium]-bis(4-methoxy-6-nitro) benzene sulfonic acid hydrate (XTT) assay was purchased from Biological Industries, Israel. 96-well plates were purchased from Greiner Bio-One, Germany. 6-well plates were purchased from Orange Scientific, Belgium.

Preparation of Ag_2S nanoparticles

As an example, 2-MPA was dissolved in 75 mL of deoxygenated deionized water. The pH of the solution was adjusted to 7.5 using NaOH and CH_3COOH solutions (2M). Then 42.5 mg of $AgNO_3$ was added, the pH was readjusted to 7.5 and the solution was brought to the desired temperature (30, 50 or 90 °C). 25 mL of deoxygenated aqueous Na_2S solution was then added slowly to the reaction mixture under vigorous mechanical stirring at 5000 rpm. During the reaction, samples were taken at different time points to follow the particle growth. Prepared quantum dot solutions were washed with DI water using Amicon-Ultra centrifugal filters (3000 Da cut off) and stored in the dark at 4 °C.

The influence of reaction variables was studied in different reactions keeping the Ag concentration fixed at 2.5 mM and varying the sodium sulfide and 2MPA concentrations to achieve Ag : S ratios of 2.5, 4 and 6 and 2MPA : Ag ratios of 5 and 10.

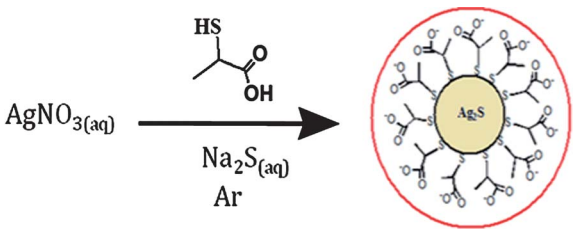

Scheme 1 Aqueous synthesis of 2-MPA coated Ag_2S NIRQDs.

Cell culture

Culturing of mouse fibroblast cells (NIH-3T3) was done according to ATCC recommendations. Cells were cultured in DMEM medium with 1.0 g L^{-1} glucose, stable L-glutamine, 3.7 g L^{-1} $NaHCO_3$, and phenol red. Full medium also contained 10% fetal bovine serum and 1% penicillin–streptomycin antibiotic solution. Trypsin–EDTA was used for cell detachment. Cells were incubated at 37 °C under 5% CO_2.

Evaluation of cytotoxicity

XTT assay was used for the evaluation of cytotoxicity. 10 000 cells per well in 96-well plates were seeded. Following overnight incubation, the medium was replenished; cells were treated with QDs (10 to 600 μg mL^{-1}) and incubated for 24 h. After washing, XTT reaction solution was added and incubated for 2 h. Spectrophotometric readings were taken at 500 and 650 nm. Absorbance at 650 nm was subtracted from the absorbance at 500 nm which corrects the results for the QD absorbance. For each sample, six replicates were used from two independent experiments. The statistical significance of the observed differences was determined using one-way ANOVA with Tukey's multiple comparison test of the GraphPad Prism software package from GraphPad Software, Inc., USA.

Cell imaging

50 000 cells per well in 6-well plates containing cover glasses were seeded. After overnight incubation, cells were treated with 200 μg mL^{-1} QDs in full medium for 24 h. Following the washing step, cells were fixed with 4% paraformaldehyde. A Zeiss LSM 510 confocal laser scanning microscope equipped with a Plan-Neofluar 40X (NA: 1.3) objective was used for image acquisition. The excitation wavelength was 543 nm. A LP605 filter was used to collect QD emission.

Characterization methods

Absorbance spectra were taken with a Shimadzu 3101 PC UV-vis-NIR spectrometer in the 300–1000 nm range. Particle sizes were calculated from the experimentally measured absorption edge by using the Brus equation[33,34] (eqn 1):

$$\Delta E = \frac{\hbar^2\pi^2}{8R^2}\left[\frac{1}{m_e}+\frac{1}{m_h}\right] - 1.8\frac{e^2}{\varepsilon_{Ag_2S}\,4\pi\varepsilon_0 R} \quad (1)$$

where ΔE is the band gap energy difference between the bulk semiconductor and the nanocrystal, R is the radius of the nanocrystal, m_e (0.286 m_0) and m_h (1.096) are the effective electron and hole masses for Ag_2S, respectively,[26] and ε_{Ag_2S} (5.95) is the dielectric constant.[26]

In the photoluminescence (PL) measurements, Ag_2S-2MPA samples were excited with a continuous-wave, frequency-doubled Nd:vanadate laser operating at 532 nm. The excitation beam was chopped at 24 Hz to provide a reference for lock-in detection. The emitted luminescence was then collected with a concave gold reflector and imaged into a 0.5 m Czerny-Turner monochromator. An amplified silicon detector sensitive over the wavelength range of 400–1100 nm was used together with a lock-in amplifier. The excess pump light was blocked by using a long-pass filter that had a transmission of 90% from 550 to 1100 nm. In the determination of the luminescence bands, the spectral response of the detection system was also taken into account. For quantum yield (QY) calculations, samples were prepared at five different concentrations and LDS 798 NIR dye in methanol (quantum yield reported as 14% by the producer) was used as a reference. QY calculations were done based on the procedures detailed in the literature.[35–37]

A few mL of the Ag_2S-2MPA solutions were freeze-dried for X-PS, X-RD and ATR-FTIR analysis. A Thermo Scientific K-Alpha XPS with Al Kα monochromatic radiation (1486.3 eV) was used for the XPS analysis of Ag_2S nanoparticles. Powdered samples were placed on an aluminum adhesive tape. 50.0 eV pass energy was used for the scans with a flood gun. A 400 μm spot size was used. A base pressure of greater than 3×10^{-9} mbar and experimental pressure of 1×10^{-7} mbar were achieved. The C 1s peak at 285.0 eV was used as a reference. For XRD measurements, the powdered sample was placed on a piece of glass with double sided sticky tape. Tape was attached to a sample holder with dough. A D8 Advance Bruker instrument with Cu Kα radiation ($\lambda = 1.5406$ Å) was used for the crystal pattern analysis between 2θ angles of 10° and 80°. Infrared spectra were taken with a Thermoscientific Nicolet iS10 instrument (ATR-FTIR) in the wavenumber range of 400–4000 cm^{-1}.

TEM images were taken on a Tecnai G2 Spirit BioTwin Transmission Electron Microscope with a single-tilt specimen holder (FEI Company) operated at 120 kV. Samples were prepared by dropping a dilute Ag_2S-2MPA colloidal solution onto a carbon coated copper grid and allowing to dry.

A Malvern Zetasizer Nano S (red badge) ZEN 1600 was used for the measurement of the hydrodynamic size of aqueous nanoparticles.

The zeta potential of the colloidal solutions was measured with a Brookhaven ZetaPALS zeta potential analyzer instrument by using the Smoluchowsky model.

A Spectro Genesis FEE Inductively Coupled Plasma Optical Emission Spectrometer (ICP OES) was used for the determination of Ag concentration in solutions. QDs were digested with acids and diluted to certain volumes. Ag^+ ion concentrations in solutions were determined by correlating a regressed standard curve.

Results and discussions

Synthesis and characterization of 2MPA coated Ag_2S NIRQDs

2MPA coated Ag_2S QDs were prepared in water with slow addition of sulfide to a 2MPA–silver salt mixture. The color of the solution turned yellow with the addition of sulfide ion and the resulting colloidal QD solution had a dark brown color.

The crystal structure of the formed nanoparticles was investigated by powder XRD. A broad XRD spectrum was recorded for the as-made Ag_2S-2MPA nanoparticles as seen in Fig. 1, similar to those reported by Jiang *et al.*[29] The nano size of the particles causes peak broadening and the amorphous coating hides the crystal peaks. After samples were heated up to 180 °C over 1 h under Ar atmosphere, sharp identifiable peaks were obtained in the XRD spectrum (Fig. 1b). The coating material may decompose or detach from the nanoparticle surface, and particles may grow at 180 °C providing a well resolved pattern. The obtained pattern corresponds to the monoclinic α-Ag_2S XRD pattern (stable crystal form at ambient atmosphere) having JCPDS no. 14-72 (according to STOE WinXPOW software) which is in agreement with previous reports.[29,32]

The IR spectrum of Ag_2S-2MPA confirms the binding of 2MPA from the thiol since there is no S–H stretching band around 2560 cm^{-1}, but confirms the presence of 2MPA (Fig. 2). Strong bands at 1560 and 1390 cm^{-1} are typical for the asymmetric and symmetric stretching modes of carboxylate, and the peaks at 2968 cm^{-1} and 2928 cm^{-1} are assigned to the asymmetric and symmetric C–H stretching of 2MPA.

XPS of Ag_2S-2MPA QDs confirmed the chemical structure. Fig. 3 shows the Ag 3d and S 2p core level peaks of Ag_2S. Binding energies (BE) of the Ag $3d_{5/2}$ and $3d_{3/2}$ spin-orbit pair appear at 367.5 eV and 373.5 eV (level 0: no etching) (Table 1 and Fig. 3), which agrees well with the literature values for Ag_2S.[38,39] These

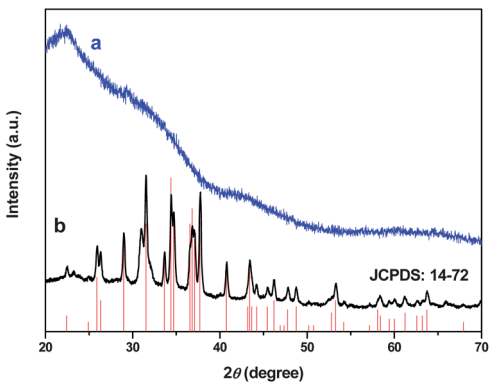

Fig. 1 XRD patterns of Ag_2S QDs (a) at room temperature and (b) after 180 °C heat treatment.

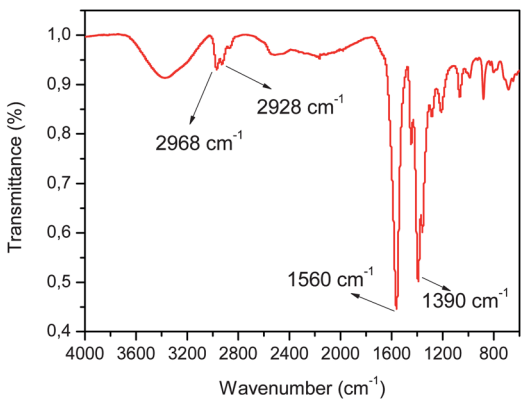

Fig. 2 IR spectrum of 2MPA coated Ag_2S QDs.

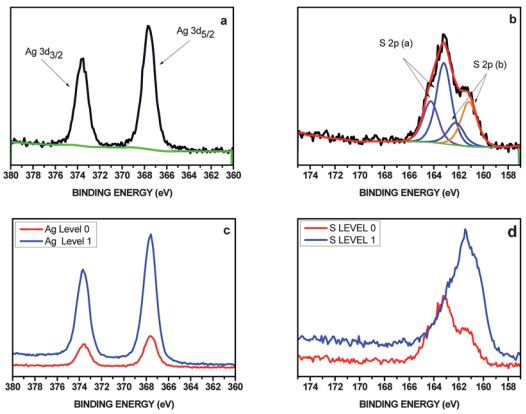

Fig. 3 (a) Ag 3d and (b) S 2p XPS spectra of Ag_2S-2MPA QDs before etching. Comparison of (c) Ag 3d and (d) S 2p peaks before (level 0) and after (level 1) plasma etching.

Table 1 Binding energies of Ag and S core levels

	Peak	BE (eV)	FWHM	%Area
Level 0				
	$Ag\ 3d_{5/2}$	367.49	1.44	20.93
	$Ag\ 3d_{3/2}$	373.51	1.44	
	$S\ 2p_{3/2}$	161.00	1.69	33.1
	$S\ 2p_{1/2}$	162.06	1.69	
	$S\ 2p_{3/2}$	162.93	1.31	45.98
	$S\ 2p_{1/2}$	164.13	1.31	
Level 1				
	$Ag\ 3d_{5/2}$	367.66	1.34	20.07
	$Ag\ 3d_{3/2}$	373.66	1.34	
	$S\ 2p_{3/2}$	160.41	1.25	9.25
	$S\ 2p_{1/2}$	161.47	1.25	
	$S\ 2p_{3/2}$	161.58	2.4	20.63
	$S\ 2p_{1/2}$	162.84	2.4	

signals shifted to 367.7 eV and 373.7 eV when the surface was etched by Ar^+ plasma (level 1). The difference between the levels can be seen in Fig. 3c. The S 2p core level could be fitted to two different spin-orbit coupling pairs (Fig. 3b). The S $2p_{3/2}$ peak at 161 eV is indicative of an Ag–S–Ag bond and the second S $2p_{3/2}$ peak at 163 eV is due to the thiol of the capping agent (2MPA).[38,40] Depth analysis through plasma etching supports such a peak assignment. As can be seen in Fig. 3d, the peak at around 163 eV diminished and two peaks at 160.41 and 161.58 eV dominated the S 2p core level spectrum after etching. Both of these peaks are due to core Ag_2S, but upon etching slight differences in the chemical environment may occur, causing such a slight shift in the peak position. Area analysis of the peaks indicates a sulfur rich surface and a major contribution from 2MPA (Tables 1 and 2). Upon etching, the Ag : S ratio reaches the theoretical value of 2 and the ratio of sulfur from Ag–S to sulfur from 2MPA increases (Table 2).

Influence of reaction variables on particle properties

Ag_2S-2MPA quantum dots have a near band-edge emission (Fig. 4). The particle size and properties can be tuned with reaction temperature, and ligand : Ag and Ag : S ratios. Changing such parameters changed the crystal size of the

Table 2 Atomic ratios of Ag and S by XPS analysis

	$Ag : S_{Ag-S}$	$Ag : S_{total}$	$S_{Ag-S} : S_{2MPA}$
Level 0	0.632	0.265	1.39
Level 1	2.170	0.672	2.23

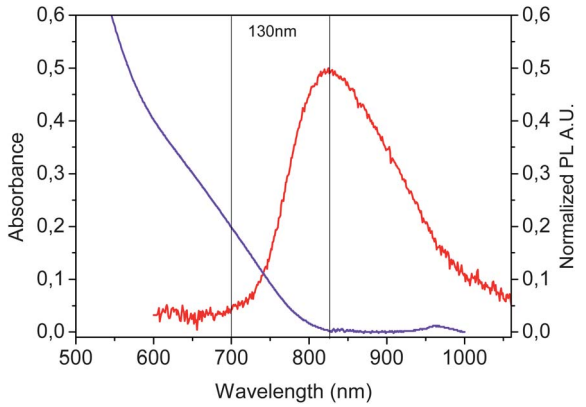

Fig. 4 Absorbance and photoluminescence spectra of Ag_2S QDs (Ag : S = 4, 2MPA : Ag = 5, T = 50 °C, 7 h reaction).

particles between 2.3 and 3.05 nm with hydrodynamic sizes up to 4.7 nm (Table 3, Fig. S1†). Hydrodynamic sizes measured by DLS are larger than the calculated crystal sizes due to the presence of the thin organic coating (2MPA) on the nanocrystals. All the colloidal particles have a negative surface potential at and above −30 eV, as expected from the carboxylate groups on the surface, which supports colloidal stability. Luminescence peaks are rather broad with FWHM around 160 nm, but this is usual for aqueous preparations.[28,29,41]

One of the most significant parameters affecting crystal growth and hence properties is the reaction temperature.

Quantum confined Ag_2S particles could be easily synthesized at 30, 50, and 90 °C (Table 3). Typical absorbance and PL spectra of the Ag_2S QDs, synthesized at different temperatures are shown in Fig. 5. Increasing the temperature causes a red shift in the absorption onset, indicating an increase in crystal size with increasing temperature from 2.38 to 2.7 nm, which is in agreement with the literature.[3,29] Usually, the critical size for stable particles increases with temperature, causing the formation of larger crystals at higher temperatures. In this case, the most significant change is seen at 90 °C. Also, other than a dramatic difference in the particle size, a significant improvement (30%) in the luminescence was observed on increasing the reaction temperature from 30 to 50 °C (Fig. 5). This might be due to better crystallization of the particles at 50 °C.

The growth of particles with time was monitored at these three temperatures. For the highest possible luminescence intensity, the optimum reaction duration was determined to be 3 h at 90 °C, 7 h at 50 °C and 24 h at 30 °C (Fig. S2 and S3†). Absorbance and PL spectra of the aliquots taken from the reaction at 50 °C from the first hour of the reaction until 22 h are shown in Fig. 6. The photoluminescence quantum yield (PLQY) of the NIRQDs at 7 h is 27%. At longer reaction times, significant peak broadening was observed. As can be seen in Fig. 6, there is a clear red shift in

Table 3 Influence of Ag : S, 2MPA : Ag and reaction temperature on the properties of Ag_2S-2MPA QDs

Ag : S	2MPA : Ag	Temp. (°C)	Rxn time (h)	λ_{cutoff}[a] (nm)	Size[b] (nm)	Band gap (eV)	$\lambda_{em,max}$ (nm)	FWHM (nm)	D_h[c] (nm)	Zeta pot. (mV)	QY (%)[d]
4	5	30	3	727	2.38	1.71	837	157	3.3	−30	—
4	5	30	1	695	2.29	1.79	827	157	2.8	−55	—
4	5	50	3	757	2.46	1.64	827	173	3.1	−39	—
4	5	90	3	834	2.70	1.49	851	181	3.1	−57	17
4	10	90	3	935	3.05	1.33	950	—	3.9	−46	—
4	10	30	1	711	2.33	1.75	815	162	3.0	−42.3	7
2.5	5	90	3	950–990	>3.1	<1.3	—	—	4.7	−58	—
6	5	90	3	763	2.48	1.63	828	168	3.1	−77.5	14
6	5	30	1	655	2.20	1.9	786	220	3.0	−55	—

[a] Absorbance onset. [b] Calculated by Brus equation. [c] Hydrodynamic diameter measured by DLS and reported as the number average. [d] Quantum yield calculated with respect to LDS 798 near-IR dye.

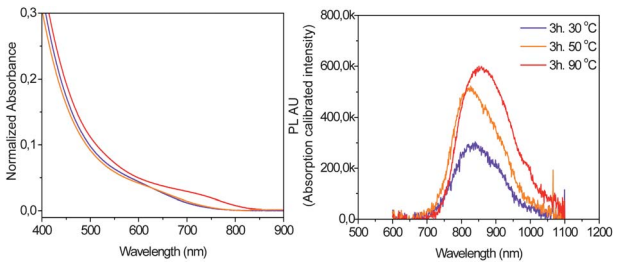

Fig. 5 Absorbance and photoluminescence spectra of the Ag_2S-2MPA particles prepared at different reaction temperatures (Ag : S = 4, 2MPA : Ag = 5).

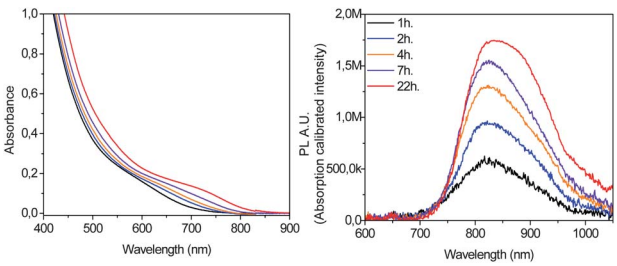

Fig. 6 Time dependent evolution of (a) absorbance and (b) photoluminescence bands for the reaction at 50 °C (Ag : S = 4 and 2MPA : Ag = 5).

the absorbance onset with time. On the other hand, the emission peak did not show any shift at the high energy end, but a broadening and a slight shift at the low energy tail. The red shift in both of these spectra confirms the increase in particle size with time. However, it appears to be more like an increase in size distribution as opposed to a complete growth of all particles. This observation can be investigated further in future.

Changing the 2MPA : Ag ratio can contribute to colloidal stability, particle size control and luminescence efficiency. Usually, increasing the coating : cation ratio leads to a decrease in the particle size. However, in the Ag_2S-2MPA system, a different trend was seen. 2MPA : Ag molar ratios of 5 and 10 were studied in reactions performed at 90 and 30 °C. At 90 °C, doubling the 2MPA : Ag ratio increased the particle size from 2.70 to 3.05 nm with an approximately 100 nm red shift in the emission peak, which was also accompanied by a dramatic decrease in the luminescence intensity (Table 3 and Fig. 7a). Since the band edge of the Si detector used restricts the measurements beyond 1000 nm, it is difficult to discuss the PL properties of the larger particles (3 nm). On the other hand, increasing 2MPA : Ag ratio at 30 °C did not change the particle properties as much. The major effect of increasing the amount of 2MPA at 30 °C is actually better luminescence which is centered around 820 nm (Fig. 7b). More coating may provide better surface passivation and less surface defects. This may reduce non-radiative coupling events, and therefore increase the luminescence efficiency. The major difference in properties originating from the reaction temperature actually depends on the stability of 2MPA. When 2MPA was heated above 50 °C in water under conditions identical to the QD synthesis, a yellow color appeared after 4 h, indicating decomposition and sulphur release. This has two consequences: (1) as the 2MPA amount increases, there will be more sulphur release, decreasing the Ag : S ratio, and therefore increasing the particle size (Fig. 7a); (2) 2MPA decomposition would decrease the effective thiol binding and interfere with the surface passivation. This may cause surface trap related non-radiative couplings and hence poorer luminescence. Less effective surface passivation may also lead to the formation of larger particles. The reactions at 90 °C are not reproducible above 3 h due to excessive 2MPA decomposition.

Interestingly, for the particles prepared at room temperature a substantial increase in the PLQY was observed over time which was not seen in case of 2MPA coated CdS.[41] Fig. 8 shows the red shift in absorbance edge from the first day to 6 months after the synthesis. Luminescence intensity increased dramatically within the first month by up to 39%, and then decreased. These changes brought about a decrease in the zeta potential as well. Particle properties are given in Table 4. This event is under investigation, but slow decomposition of 2MPA may deposit more sulphur to the surface and cause a slight particle growth and improve luminescence by pacifying surface traps. However, this may eventually cause more traps on the surface as well which would have a negative impact on PLQY.

The stoichiometry of silver to sulphide ions influences the optoelectronic properties (emission tunability) and particle sizes of the Ag_2S-2MPA QDs dramatically. Three different Ag : S ratios (2.5, 4, and 6) were studied at 90 °C (Table 3) keeping the other variables constant. Decreasing the Ag : S ratio from 6 to

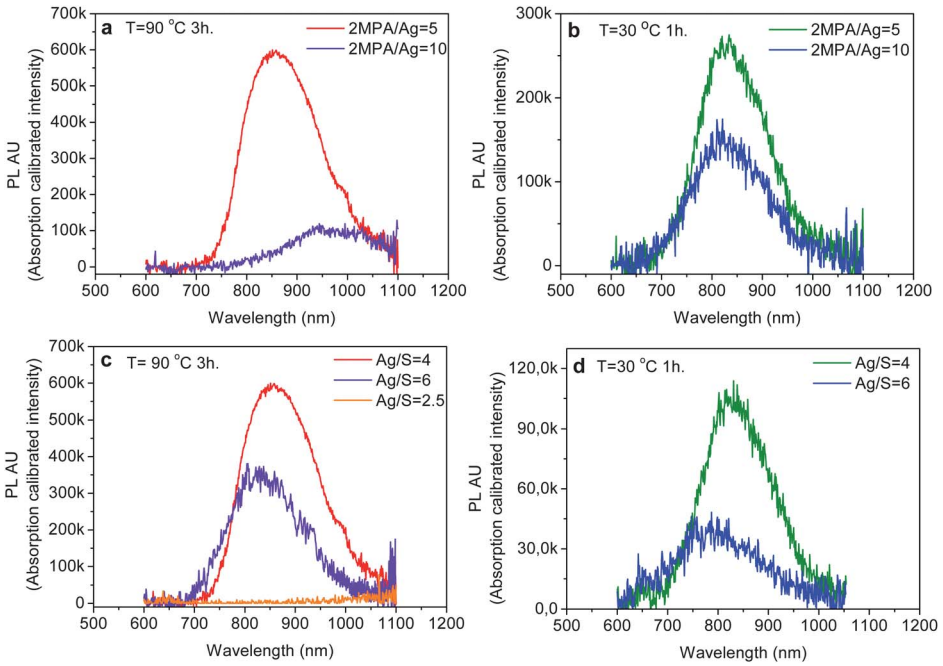

Fig. 7 PL spectra of Ag_2S QDs prepared at different 2MPA : Ag ratios at (a) 90 °C and (b) 30 °C, and at different Ag : S ratios at (c) 90 °C and (d) 30 °C.

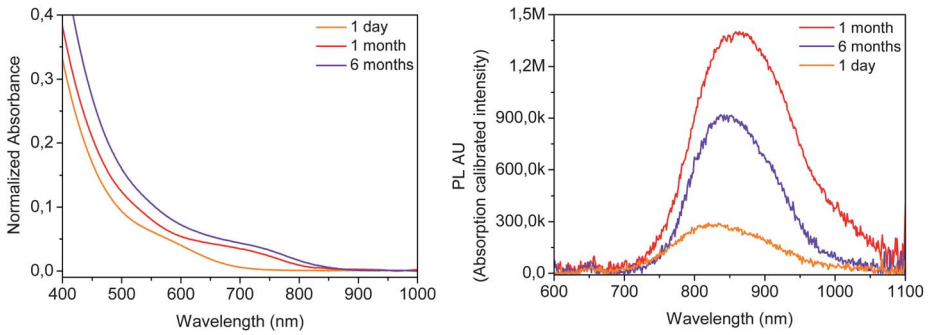

Fig. 8 Absorbance and PL spectra of Ag_2S-2MPA NIRQDs (synthesized at room temperature) recorded after the synthesis.

Table 4 Changes in the particle properties with time

Analysis time[e]	Ag : S	2MPA : Ag	λ_{cutoff}[a] (nm)	Size[b] (nm)	Band gap (eV)	$\lambda_{em,max}$ (nm)	FWHM (nm)	D_h[c] (nm)	Zeta pot. (mV)	QY[d] %
1 day	4	5	695	2.29	1.79	827	157	2.8	−55	<5
1 month	4	5	822	2.66	1.51	863	165	3.5	−38	39
6 months	4	5	855	2.77	1.45	843	141	4.3	−28	29

[a] Absorbance onset. [b] Calculated by Brus equation. [c] Hydrodynamic diameter measured by DLS and reported as the number average. [d] Quantum yield calculation with respect to LDS 798 near IR dye. 1 h reaction. [e] Time passed after synthesis.

2.5 causes a red shift in the absorbance and luminescence spectra, indicating the formation of larger particles. At the ratio of 2.5, QDs with only a very poor luminescence signal with a peak maximum over 1000 nm (which was the limit of our detector, Fig. 7c) were obtained. In such a result, as much as the stoichiometry, some decomposition of 2MPA may have played a role as well. Particles prepared at 90 °C are larger than those synthesized at lower temperatures as discussed before (Table 3). Increasing the Ag : S ratio decreased the particle size at 30 °C as well (Fig. 7d and Table 3). The best quality particles are obtained at the Ag : S ratio of 4.

In vitro characterization

The cytotoxicity of Ag_2S-2MPA QDs was tested on NIH-3T3 mouse fibroblast cells using XTT assay,[42] which is based on

mitochondrial reductase enzyme activity. The aqueous Ag_2S-2MPA used for these studies had a concentration of 2.5 mg particles per mL, which corresponds to 1.3 mg silver per mL (measured by ICP OES), and had 10% PLQY six months after preparation at the time of cell studies.

Fig. 9 shows the percentage change in metabolic activity of control and Ag_2S treated cells as a function of QD concentration between 10 to 600 μg particles per mL after 24 h incubation. Statistical analysis of the results indicates no significant difference in the vitality of untreated and Ag_2S treated samples. This result is in line with previous reports stating low or no toxicity for silver complexes, unlike free silver ions.[43–45] The biocompatibility of silver sulfide quantum dots is also supported by other studies.[43] What was not seen before was the cytocompatibility at such high doses of Ag_2S. Suresh and Pelletier *et al.* biofabricated Ag_2S nanoparticles using the metal-reducing bacterium *S. oneidensis*, and observed no cytotoxicity at 150 μg mL^{-1} and below on epithelial and macrophage cells after 12 h treatment. Silver sulfide nanoworms prepared in BSA have also been shown to have low toxicity on HeLa cervical cancer cells up to a 50 μg mL^{-1} dose. However, cells did proliferate at higher doses (0.2–1 g mL^{-1}), since protein BSA acts as a nutrient for many cells.[46] There are no nanoparticles in the literature which are cytocompatible at such high doses (600 μg particles per mL or 312 μg Ag per mL), to the best of our knowledge. Also, considering that NIH-3T3 is usually more vulnerable than cancer cell lines, this is an extremely valuable finding.

We also studied the cellular uptake and intracellular localization of Ag_2S-2MPA using confocal laser scanning microscopy. To the best of our knowledge, this is the first fluorescence microscopy study of a mammalian cell imaged with a Ag_2S QD. NIH-3T3 cells were treated with 200 μg particles per mL QDs for 24 h and fixed with paraformaldehyde before image acquisition. Ag_2S-2MPA NIRQDs are effectively internalized and exhibit a punctuated cytoplasmic distribution indicating localization to endosomes and lysosomes, as is typical for QD nanoparticles

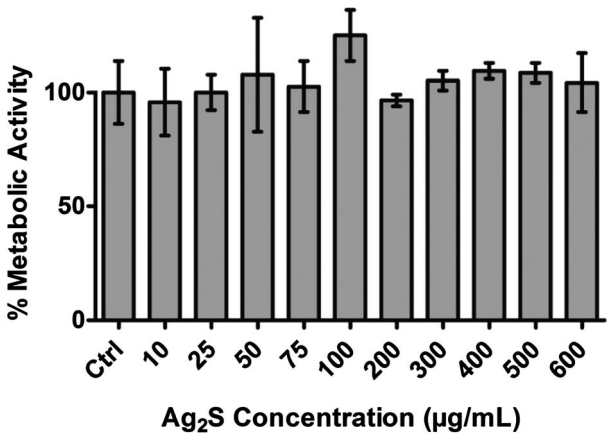

Fig. 9 Change in the metabolic activity of NIH/3T3 mouse fibroblast cells after 24 h exposure to Ag_2S quantum dots as determined by XTT assay. Reported values are mean ± SEM ($n = 6$). No significant difference was observed between control (Ctrl) and QD treated cells (one-way ANOVA with Tukey's multiple comparison at $p < 0.05$).

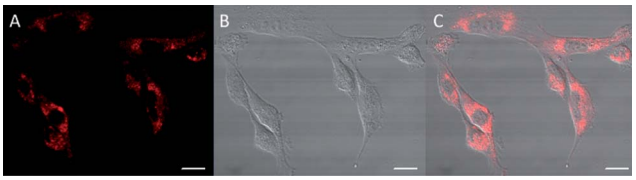

Fig. 10 Cellular uptake and localization of Ag_2S QDs by NIH/3T3 mouse fibroblast cells (200 μg mL^{-1} QDs, 24 h incubation). (A) Fluorescence, (B) transmission and (C) overlay channels of the confocal micrograph. The scale bar represents 20 μm.

(Fig. 10). As expected for a particle of this size, no nuclear localization is observed.

Infra-red emission of the particles provides a major advantage in the cell imaging studies. The autofluorescence of the cells is particularly strong in the green region of the electromagnetic spectrum. Therefore, infra-red fluorescence imaging is ideal since there is minimal or no background signal from the cells in this region. However, typical confocal fluorescence Photo Multiplier Tube (PMT) detectors have low sensitivity in this region, resulting in reduced photon collection. To overcome this difficulty, we increased the laser power and detector sensitivity to the maximum allowed level in our system. Using these settings, we could obtain high quality confocal images with a clean background.

Conclusions

Colloidally stable, highly cytocompatible and highly luminescent aqueous Ag_2S NIR emitting QDs were successfully synthesized in water with a 2MPA coating. The size and therefore the emission wavelength of these NIRQDs can be tuned by varying the Ag : S and 2MPA : Ag ratios and the reaction temperature. Decomposition of 2MPA at 90 °C at extended reaction times impacts the crystal size. Particle size can be tuned between 2.3 and 3.1 nm with an emission maximum between 780 and 950 nm. The particles demonstrate a strong negative zeta potential due to the carboxylate groups on the surface and have exhibited excellent colloidal stability for over a year now. These particles possess significantly better PLQY in the range of 7–39% compared to reported values in the literature, which are less than 1% for Ag_2S.[28,29,31]

In addition, these Ag_2S-2MPA NIRQDs showed dramatically improved cytocompatibility in NIH/3T3 cell lines and have been demonstrated as effective imaging agents for the first time in the literature. Excellent cytocompatibility, improved QY and colloidal stability make these nanoparticles an exciting candidate for bio-applications, specifically for *in vivo* imaging. These NIRQDs are also invaluable for solar energy conversion with strong absorption and emission characteristics.

Acknowledgements

The authors thank Koc University and TUBITAK (Project no: 109R031) for the funding, KUYTAM and Dr Uğur Unal at Koc University for XRD, and Seckin Ozturk and Tugba Endogan at METU Central Laboratory for TEM.

Notes and references

1 H. M. E. Azzazy, M. M. H. Mansour and S. C. Kazmierczak, *Clin. Biochem.*, 2007, **40**, 917–927.
2 H. S. Mansur, *Wiley Interdiscip. Rev.: Nanomed. Nanobiotechnol.*, 2010, **2**, 113–129.
3 Y. He, Y. Zhong, Y. Su, Y. Lu, Z. Jiang, F. Peng, T. Xu, S. Su, Q. Huang, C. Fan and S.-T. Lee, *Angew. Chem., Int. Ed.*, 2011, **50**, 5695–5698.
4 W. Jiang, A. Singhal, J. Zheng, C. Wang and W. C. W. Chan, *Chem. Mater.*, 2006, **18**, 4845–4854.
5 A. Guchhait, A. K. Rath and A. J. Pal, *Sol. Energy Mater. Sol. Cells*, 2011, **95**, 651–656.
6 W. Jiang, A. Singhal, B. Y. S. Kim, J. Zheng, J. T. Rutka, C. Wang and W. C. W. Chan, *J. Assoc. Lab. Autom.*, 2008, **13**, 6–12.
7 E. İ. Altınoğlu and J. H. Adair, *Wiley Interdiscip. Rev.: Nanomed. Nanobiotechnol.*, 2010, **2**, 461–477.
8 P. Sharma, S. Brown, G. Walter, S. Santra and B. Moudgil, *Adv. Colloid Interface Sci.*, 2006, **123–126**, 471–485.
9 R. Aswathy, Y. Yoshida, T. Maekawa and D. Kumar, *Anal. Bioanal. Chem.*, 2010, **397**, 1417–1435.
10 Y. Taik Lim, S. Kim, A. Nakayama, N. E. Stott, M. G. Bawendi and J. V. Frangioni, *Mol. Imaging*, 2003, **2**, 50–64.
11 J. V. Frangioni, *Curr. Opin. Chem. Biol.*, 2003, **7**, 626–634.
12 P. P. Ghoroghchian, M. J. Therien and D. A. Hammer, *Wiley Interdiscip. Rev.: Nanomed. Nanobiotechnol.*, 2009, **1**, 156–167.
13 S. B. Rizvi, S. Ghaderi, M. Keshtgar and A. M. Seifalian, Semiconductor quantum dots as fluorescent probes for *in vitro* and *in vivo* bio-molecular and cellular imaging, *Nano Rev.*, 2010, **1**: 5161.
14 C.-A. J. Lin, T. Liedl, R. A. Sperling, M. T. Fernandez-Arguelles, J. M. Costa-Fernandez, R. Pereiro, A. Sanz-Medel, W. H. Chang and W. J. Parak, *J. Mater. Chem.*, 2007, **17**, 1343–1346.
15 V. Biju, S. Mundayoor, R. V. Omkumar, A. Anas and M. Ishikawa, *Biotechnol. Adv.*, 2010, **28**, 199–213.
16 L. Guo-Xi, G. Miao-Miao, Z. Jian-Rong and Z. Jun-Jie, *Nanotechnology*, 2009, **20**, 415103.
17 H. Y. Chen, S. S. Cui, Z. Z. Tu, J. Z. Ji, J. Zhang and Y. Q. Gu, *Photochem. Photobiol.*, 2011, **87**, 72–81.
18 B. Blackman, D. Battaglia and X. Peng, *Chem. Mater.*, 2008, **20**, 4847–4853.
19 N. Y. Morgan, S. English, W. Chen, V. Chernomordik, A. Russo, P. D. Smith and A. Gandjbakhche, *Acad. Radiol.*, 2005, **12**, 313–323.
20 S. Kim, Y. T. Lim, E. G. Soltesz, A. M. De Grand, J. Lee, A. Nakayama, J. A. Parker, T. Mihaljevic, R. G. Laurence, D. M. Dor, L. H. Cohn, M. G. Bawendi and J. V. Frangioni, *Nat. Biotechnol.*, 2004, **22**, 93–97.
21 H. Ding, K.-T. Yong, W.-C. Law, I. Roy, R. Hu, F. Wu, W. Zhao, K. Huang, F. Erogbogbo, E. J. Bergey and P. N. Prasad, *Nanoscale*, 2011, **3**, 1813–1822.
22 Y. Du, B. Xu, T. Fu, M. Cai, F. Li, Y. Zhang and Q. Wang, *J. Am. Chem. Soc.*, 2010, **132**, 1470–1471.
23 R. Xie, K. Chen, X. Chen and X. Peng, *Nano Res.*, 2008, **1**, 457–464.
24 K.-T. Yong, I. Roy, R. Hu, H. Ding, H. Cai, J. Zhu, X. Zhang, E. J. Bergey and P. N. Prasad, *Integr. Biol.*, 2010, **2**, 121–129.
25 O. Madelung, *Semiconductors: Data Handbook*, Springer Verlag, Berlin Heidelberg Newyork, 2004, p. 1528.
26 S. H. Ehrlich, *J. Imaging Sci. Technol.*, 1993, **37**, 73–91.
27 M. P. Hirsch, *Environ. Toxicol. Chem.*, 1998, **17**, 601–604.
28 M. Yarema, S. Pichler, M. Sytnyk, R. Seyrkammer, R. T. Lechner, G. Fritz-Popovski, D. Jarzab, K. Szendrei, R. Resel, O. Korovyanko, M. A. Loi, O. Paris, G. N. Hesser and W. Heiss, *ACS Nano*, 2011, **5**, 3758–3765.
29 P. Jiang, Z.-Q. Tian, C.-N. Zhu, Z.-L. Zhang and D.-W. Pang, *Chem. Mater.*, 2011, **24**, 3–5.
30 A. Sahu, L. Qi, M. S. Kang, D. Deng and D. J. Norris, *J. Am. Chem. Soc.*, 2011, **133**, 6509–6512.
31 Y.-P. Gu, R. Cui, Z.-L. Zhang, Z.-X. Xie and D.-W. Pang, *J. Am. Chem. Soc.*, 2011, **134**, 79–82.
32 G. A. Martínez-Castañón, M. G. Sánchez-Loredo, H. J. Dorantes, J. R. Martínez-Mendoza, G. Ortega-Zarzosa and F. Ruiz, *Mater. Lett.*, 2005, **59**, 529–534.
33 L. E. Brus, *J. Chem. Phys.*, 1984, **80**, 4403–4409.
34 L. Brus, *J. Phys. Chem.*, 1986, **90**, 2555–2560.
35 A Guide to Recording Fluorescence Quantum Yields, http://www.horiba.com/fileadmin/uploads/Scientific/Documents/Fluorescence/quantumyieldstrad.pdf.
36 S. Celebi, A. K. Erdamar, A. Sennaroglu, A. Kurt and H. Y. Acar, *J. Phys. Chem. B*, 2007, **111**, 12668–12675.
37 H. Li, W. Y. Shih and W.-H. Shih, *Ind. Eng. Chem. Res.*, 2007, **46**, 2013–2019.
38 R. Chen, N. T. Nuhfer, L. Moussa, H. R. Morris and P. M. Whitmore, *Nanotechnology*, 2008, **19**, 455604.
39 R. B. C. Orléans, http://www.lasurface.com/database/elementxps.php.
40 *Handbook of the Elements and Native Oxides*, http://www.xpsdata.com/XI_BE_Lookup_table.pdf.
41 H. Y. Acar, R. Kas, E. Yurtsever, C. Ozen and I. Lieberwirth, *J. Phys. Chem. C*, 2009, **113**, 10005–10012.
42 D. A. Scudiero, R. H. Shoemaker, K. D. Paull, A. Monks, S. Tierney, T. H. Nofziger, M. J. Currens, D. Seniff and M. R. Boyd, *Cancer Res.*, 1988, **48**, 4827–4833.
43 A. K. Suresh, M. J. Doktycz, W. Wang, J. W. Moon, B. Gu, H. M. Meyer III, D. K. Hensley, D. P. Allison, T. J. Phelps and D. A. Pelletier, *Acta Biomater.*, 2011, **7**, 4253–4258.
44 O. Choi, T. E. Clevenger, B. Deng, R. Y. Surampalli, L. Ross, Jr. and Z. Hu, *Water Res.*, 2009, **43**, 1879–1886.
45 S. A. Blaser, M. Scheringer, M. MacLeod and K. Hungerbühler, *Sci. Total Environ.*, 2008, **390**, 396–409.
46 R. Xing, S. Liu and S. Tian, *J. Nanopart. Res.*, 2011, 4847–4854.